RIGID WHEEL DESIGN AND EVALUATION FOR LIGHTWEIGHT SNOW ROVER

Austin Lines^a, Joshua Elliott^b, and Laura Ray^b

^a Cold Regions Research and Engineering Laboratory, 72 Lyme Road, Hanover, NH 03755
^b Thayer School of Engineering at Dartmouth College, 14 Engineering Dr, Hanover, NH 03755
austin.lines@gmail.com, joshuajameselliott@gmail.com, laura.e.ray@dartmouth.edu

Abstract

This paper presents a design approach for rigid wheels operating in highly variable, deformable terrain to improve the mobility, reliability, and efficiency of an autonomous vehicle driving on snow. The longstanding Bekker-Wong theory of terramechanics is used as the basis for the design changes with the wide range of terrain parameters for snow serving as inputs to the models and bounds for the problem. Modifications to the wheel width and diameter are evaluated based on their impacts to the rover as a system, with their effects on torque and drawbar pull being weighed against the resultant modifications in component sizing, rover weight, and energy use. Other factors, not included in the Bekker-Wong models but studied in single-wheel testbed experiments, such as bulldozing resistance and the observed dynamic effects of slip-sinkage, were also considered in the design decisions for the new wheel. Finally, to test these theories and assess the mobility improvements of the new design *in situ*, a four-wheeled rover, *FrostyBoy*, was developed for the new wheels and trialed in unmodified snow. While qualitatively showing an improvement in mobility on the Greenland ice sheet, the tests also uncovered dynamic modes of immobilization, in low cohesion, low stiffness snow that are not accounted for in terramechanics theory and require further investigation for trafficability to be maintained in all snow conditions.

Keywords: Rigid Wheel, Snow Mobility, Autonomous Rover

1. Introduction

A rover's mobility on deformable terrain is largely dependent on the design of its tractive elements. The shape and size of its wheels or tracks combined with the terrain's ability to support the normal and shear forces applied determine whether the robot is able to gain traction. Understanding this interaction and estimating the properties of all the terrains to be encountered is therefore critical to optimizing the design of the wheels or tracks. This paper focuses specifically on the design of rigid wheels for a lightweight, automated vehicle operating in snow.

Accessing remote areas of the ice sheets of Greenland and Antarctica to collect ground truth measurements of snow temperature, albedo, and ice stratigraphy is critical in developing and refining climate models (Quincey and Luckman, 2009; Shepherd et al., 2012). Due to the difficulty, expense, and danger of using manned vehicles to travel to these sites and gather these data, there are many benefits in replacing these traverses with autonomous rovers that could tow a variety of sensors. Previous proof-of-concept rovers, *Cool Robot* and *Yeti*, were equipped with off-the-shelf pneumatic ATV tires and have shown the potential of solar-charged, battery-powered autonomous rovers to operate for extended durations in these environments while making valuable measurements of air and snow properties (Ray et al., 2014; Trautmann et al., 2009). However, intermittent immobilization of these rovers due to spatially variable terrain parameters and their relatively high ground pressure rendered them impractical for autonomous, uninterrupted traverses where they would have to maintain mobility in all snow conditions.

The fundamental concepts that serve as the foundation for a rigid wheel interacting with a deformable terrain, like snow, were introduced by Bekker and Gregory (1956) and were later expanded upon by Wong and Reece (1967a,b). The semi-empirical equations, in what is known as the Bekker-Wong model, defined the basics of how a wheel sinks into the terrain, how this sinkage resists forward motion, and how the pressure distribution below the wheel impacts its ability to gain traction and convert torque to forward velocity. As interest in sending wheeled mobile robots (WMRs) to explore other planets

increased, researchers focused on single-wheel experiments to better define the semi-empirical equations and the associated terrain parameters defining a rigid wheel's interaction with deformable terrain. In these experiments, testbeds were filled with a homogeneous terrain type, typically a type of sand or a Martian or Lunar soil simulant, and an instrumented single wheel traversed the testbed, with the wheel speed, longitudinal velocity, applied torque, and normal load being controlled and/or measured. In some studies, pressure sensors mounted within the rim of the wheel allowed for direct measurement of the shear and normal stress profiles developed under a rigid wheel (Senatore and Iagnemma, 2014; Jayakumar et al., 2014; Nagatani et al., 2009). Other studies employed transparent testbed walls and high speed cameras to track soil particle movement beneath the wheels (Senatore and Iagnemma, 2014; Moreland et al., 2012; Inotsume et al., 2019). While these updated models are shown to be more accurate for the class of vehicle being designed for ground traverses in the polar regions, values for the terrain parameters are tuned to the terrain in the testbed and none of these single-wheel studies have been performed with snow. Only the common Bekker-Wong parameters can be found in the literature for snow. In this paper, the original equations and parameter set of the Bekker-Wong model serve as the principal method by which the performance of a lightweight, small-wheeled rover in snow is evaluated. This approach is bound to be less accurate for snow, as snow is a broad term for terrains with drastically different characteristics. Even though the design of the tractive elements cannot be precisely optimized using these equations, the first goal of this paper is to outline how performance improvements can be evaluated and the design problem can be bounded by using the range of terrain parameters found in the literature and the most widely accepted terramechanics equations.

Another drawback of the single-wheel studies is their inability to account for how the dynamics of the robot operating in non-homogenous terrain can play a key role in an immobilization. Multibody dynamics simulations of autonomous rovers are common in developing navigation and path planning algorithms and understanding the behavior of WMRs in rough terrain. Commonly available software packages allow for importation of the rover's geometry from CAD and a digital elevation model (DEM) of rough terrain to better simulate the dynamics and weight distribution as the rover drives (Rivera et al., 2019). While this helps to evaluate the design of the rover's chassis and suspension, often the simulation of the interaction between the tractive elements and the terrain is overly simplistic. Even refining the wheel-terrain model with separate subroutines to input the finely tuned semi-empirical models and terrain parameters formulated in single-wheel studies still assumes terrain homogeneity (Trease et al., 2011). While Ishigami et al. (2007) found good agreement with this simulation method in matching a four-wheel testbed study in loose soil, this method does not model how the spatial variability in the terrain parameters, which can be particularly important for snow, can cause unique dynamics which can lead to immobilization. Therefore, the second goal of this paper is to show how the new wheel design, and ultimately the terramechanics models on which it was based, were put to the test *in situ* with a four wheeled rover operating on unmodified snowy terrain.

2. Terramechanics Background

To design tractive elements for a snow rover, the basics of terramechanics theory must be understood. A rover's mobility on flat, deformable terrain is defined as generating enough forward thrust at the interface between the wheels and snow surface to overcome all resistance forces. These resistance forces include wind resistance, internal friction losses, and gravity forces on a slope, but this study deals only with compaction and bulldozing resistances that result when the rover sinks into and compresses the terrain. The difference between tractive forces and resistance forces is termed drawbar pull and it serves as the quantitative indicator of a vehicle's ability to traverse a given terrain.

This discussion of terramechanics models focuses on the drawbar pull generated from rigid wheels, rather than from tracks or pneumatic tires. Track systems result in much greater frictional energy losses in the drive train compared to wheels and add significant weight and complexity to an otherwise lightweight and simple robot. Also, from tire studies on deformable terrain (Shoop et al., 2006) and observations of pneumatic tires on snow, there is no significant deformation of the ATV tires used on *Cool Robot* and *Yeti* that would lead to a patch of constant pressure. Therefore, all models presented in this section are for a rigid wheeled vehicle.

2.1. Sinkage

The interaction of rigid wheels and deformable terrain is largely based on the compression of the soil and the resultant sinkage. The amount of sinkage and the pressure distribution under the wheel determine the forces resisting the robot's motion as well as the shear stress that can be applied to the terrain to propel the robot forward. Bekker and Gregory (1956) developed an

equation to describe the relationship between pressure and sinkage observed in plate-indentation tests

$$p = \left(\frac{k_c}{b} + k_\phi\right) z^n \tag{1}$$

where p is a nonlinear function of sinkage, z, dependent on an exponent, n, with k_c being the cohesive modulus, k_ϕ being the friction modulus, and b, the wheel width. From Bekker's equation, it follows that the pressure distribution under a rigid wheel would be highest at the lowest point, directly below the axle of the wheel. Wong (2001) showed that this is not the case. In studying flow of soil underneath a driven wheel, he found that there are two regimes (Wong, 2001). In the front region, the soil actually flows forward in the direction of robot travel, and the soil beneath the rear region flows backward. Where the two failure zones meet is the location of the maximum normal pressure, which moves forward with increasing slip (Wong and Reece, 1967a). Denoting θ_2 as the angle from bottom-dead-center (BDC) at which the back end of the wheel exits the soil, θ_m as the angle from BDC at which the pressure is maximum, and θ_1 as the angle from BDC to the surface of the terrain, θ_m can be calculated from the equation

$$\theta_m = (c_1 + c_2 i)\theta_1 \tag{2}$$

where c_1 and c_2 are empirically determined coefficients and i is the slip ratio . Using this nomenclature, the pressure distribution from θ_1 to θ_m is determined according to the Bekker pressure-sinkage model (2), rewritten below in terms of θ

$$\sigma(\theta) = \left(\frac{k_c}{b} + k_\phi\right) r^n (\cos\theta - \cos\theta_1)^n \tag{3}$$

From θ_m to θ_2 , Wong and Reece (1967a) found that the normal pressure around the rim of the wheel decreased to zero, with the stress at any position in the 'rear region' matching the stress at the corresponding relative position in the 'front region'. The equation of the stress distribution below the rear region is thus

$$\sigma(\theta) = \left(\frac{k_c}{b} + k_\phi\right) r^n \left[\cos\left(\theta_1 - \left(\frac{\theta - \theta_2}{\theta_m - \theta_2}\right)(\theta_1 - \theta_m)\right) - \cos\theta_1\right]^n \tag{4}$$

A representation of this stress distribution can be seen in Fig. 1.

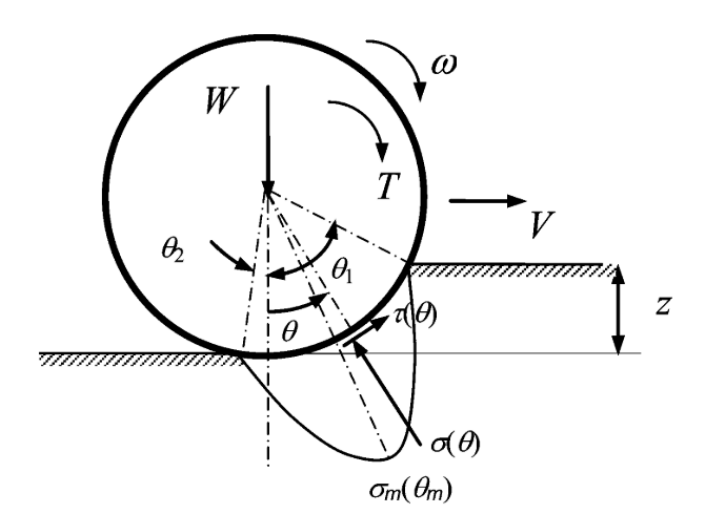


Figure 1: Stress distribution below a rigid wheel in deformable terrain (Ray, 2009)

For this analysis, c_1 and c_2 are fixed as 0.18 and 0.32, respectively, to represent low cohesion snow. No single-wheel studies have been performed to determine these parameters for snow, but these are commonly used values in the literature for modeling rigid wheels in loose, low cohesion sand (Wong and Reece, 1967a).

These equations describing pressure-sinkage curves have also been shown to fit well with homogenous terrains, such as sand (both dry and wet), sandy loam, clays, and a homogenous snowpack (Wong, 2001). But since snow is such a variable

substance, with slight changes in density, morphology, and temperature histories causing drastic changes in structure, there is no tightly controlled range of values for n, k_c , and k_ϕ in the literature. Wong (2001) references parameters that define pressure-sinkage from three studies performed in snow (the parameter values are shown in Table 1 and the resultant pressure sinkage relationships are graphically shown in Fig. 2 as curves labeled Bekker 1 through Bekker 3).

Table 1: Pressure-sinkage terrain parameters for three different types of snow for the Bekker model (Wong, 2001)

Pressure-Sinkage Parameters - Bekker Model						
Terrain Parameter	Bekker 1	Bekker 2	Bekker 3			
n	1.6	1.6	1.44			
k_c [kN/m ⁿ⁺¹]	4.37	2.49	10.55			
k_{ϕ} [kN/m ⁿ⁺²]	196.72	245.90	66.08			

Other pressure sinkage models have been proposed specifically for deep snow, which is seen to have a linear regime for small sinkage and a sharp increase in pressure as the snow compacts against a much denser layer within the snowpack. Wong and Preston-Thomas (1983) described this relationship to be

$$p(z) = k \left[-\ln\left(1 - \frac{z}{z_m}\right) \right] \tag{5}$$

where k defines the linear portion where pressure is proportional to sinkage, and z_m is the depth of the denser layer. This equation can be substituted for the Bekker model in Eq. (3) and (4) above. Similar to the parameters in the Bekker model, the two parameters in the Preston-Thomas equation also vary widely for snow. The values are presented in Table 2, with the parameters determined from measurements near Summit Station, Greenland labeled Preston 1 (Lever, 2007), and those determined from measurements on a snow-covered lake in Lebel-sur-Quévillon, Canada (described in more detail in section 4) labeled Preston 2 through Preston 5.

One can begin to understand the difficulty in encapsulating the problem of designing tractive elements for snow by looking at the splay of pressure-sinkage curves in Fig. 2 and recognizing that this only describes the results from a limited set of experiments in just one subset of terramechanics theory. While this impedes attempts to converge on an optimized wheel design, it does allow for the beginnings of defining and bounding the design challenge.

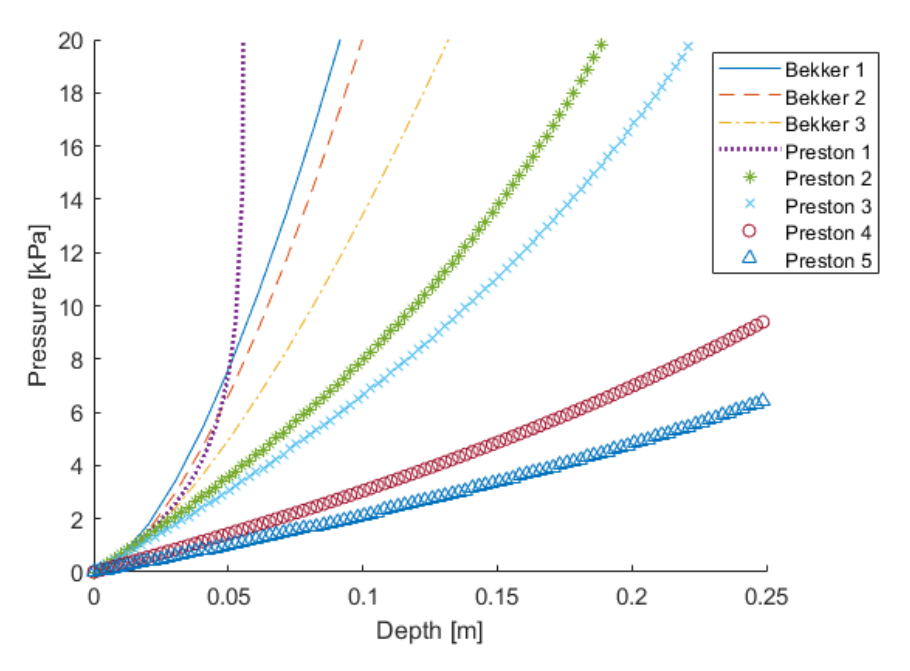


Figure 2: Range of pressure vs sinkage profiles obtained in snow.

Table 2: Pressure-sinkage terrain parameters for five different snows using the Preston-Thomas model (Wong, 2001)

Pressure-Sinkage Parameters - Preston-Thomas Model							
Terrain Parameter	Preston 1	Preston 2	Preston 3	Preston 4	Preston 5		
k [kPa/m]	59	65	56.4	27.3	19.2		
z_m [m]	0.06	0.29	0.35	0.50	0.54		

2.2. Traction

While the Bekker model describes how the terrain deforms under the weight of the robot, the shear failure of the terrain must be understood to calculate the robot's motive forces. The Mohr-Coulomb failure criterion is simple and commonly used to define the shear stress, τ , at which a soil fails

$$\tau = c + \sigma \tan \phi \tag{6}$$

where c is the cohesion of the soil, σ is the normal stress (defined by the pressure-sinkage curves above), and ϕ is the angle of internal friction. The values for cohesion and internal shearing angle of a given terrain are determined by using a shear plate or shear ring to find a relationship between shear stress and shear displacement (Wong, 2001). This relationship exhibits different characteristics depending on the terrain type. For example, Wong (2001) found that "compact sand, silt and loam, and frozen snow" show a rapid increase in shear stress with shear displacement and after quickly reaching a maximum, the shear stress drops and reaches a steady state value below its peak. This behavior can be characterized by

$$\tau = (c + \sigma \tan \phi) K_r \left\{ 1 + \left[\frac{1}{K_r \left(1 - \frac{1}{e} \right)} - 1 \right] e^{\left(1 - \frac{j}{K_\omega} \right)} \right\} \left(1 - e^{\frac{-j}{K_\omega}} \right)$$
 (7)

where j is the shear displacement, K_r is the ratio of the residual shear stress to the maximum shear stress, and K_w is the amount of shear displacement that results in the maximum shear stress (Wong, 2001). While the term 'frozen snow' is used in the terramechanics literature, a better descriptor of this type of snow, to be compatible with definitions in glaciology and snow science, is well bonded. This means that the snow crystals have undergone metamorphism that has resulted in the grains becoming connected at their boundaries, forming a three-dimensional network (Sommerfeld and LaChapelle, 1970) and can be associated with high cohesion snow. This is contrasted with what Wong (2001) calls 'fresh snow', which describes newly deposited snow that is typically unmetamorphosed with no sintering between snow crystals. However, this property is not unique to new snow, as some forms of snow metamorphosis also result in loose, disconnected snow grains (Sommerfeld and LaChapelle, 1970). Therefore, the term poorly bonded is used instead of 'fresh' to describe this type of low cohesion snow. For poorly bonded snow, Wong (2001) found the shear stress vs. shear displacement relationship to have a different shape. In this type of terrain, there is a similar sharp increase in shear stress with displacement, with further shear displacement causing the shear stress to rise and approach a steady-state, maximum value (also shown in Fig. 3). This behavior can be described by

$$\tau = (c + \sigma \tan \phi) \left(1 - e^{-j/K_s} \right) \tag{8}$$

where j is the shear displacement, and K_s is the shear deformation modulus (Wong, 2001). Shear displacement, j, along the contact patch of a rigid wheel can be calculated for both Eq. (7) and (8) for a given slip, i, according to Wong (2001)

$$j(\theta) = R_w[\theta_1 - \theta - (1 - i)(\sin \theta_1 - \sin \theta)] \tag{9}$$

From these equations and the sinkage equations from section 2.1, the shear stress acting on the contact patch of the wheel can be calculated to give a tractive force. Therefore, the shear stress-shear displacement relationships are translated to tractive force vs. slip ratio plots for rigid wheels, as shown in Fig. 3. In this plot, the weight and wheel dimensions of *Cool Robot* are used in all calculations to allow for direct comparison of the two models. Both the well bonded and the poorly bonded shear stress-shear displacement relationships are used to evaluate wheel performance of the rover since it can be expected to encounter every type of snow possible. For the well bonded condition (7), the values of K_{ω} and K_{τ} have been found to be approximately 2.2 cm and 0.66, respectively (Wong, 2001). For the poorly bonded condition (8), the value of the shear displacement modulus, K_s , has been found to be anywhere from 2.5 cm to 5 cm (Wong, 2001). As for the values of c and ϕ in the Mohr-Coulomb shear failure criterion (6), there is significant variation from experiment to experiment, most likely due to the variability of snow as a material. From the three studies referenced by Wong (2001), cohesion, c, varies from approximately 0.6 kPa to 6 kPa. The value for the angle of internal friction varies from 9° (Haehnel and Shoop, 2004) to 23°

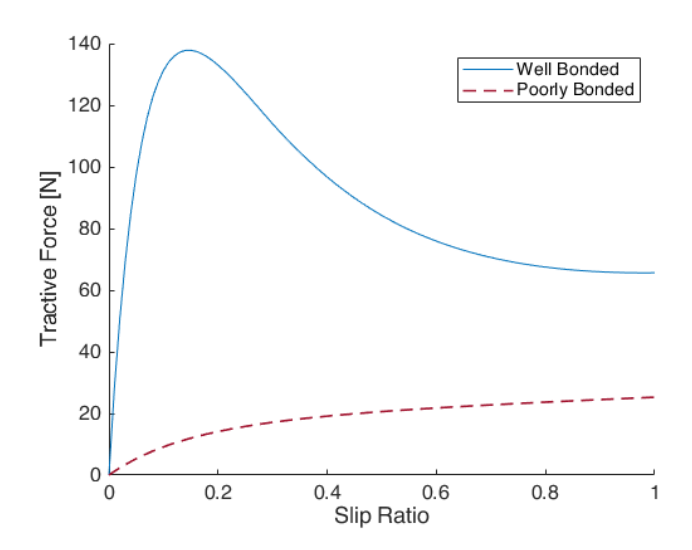


Figure 3: Comparison of well bonded (7) and poorly bonded (8) snow traction models for the two types of snow defined by the parameters in Table 3.

(Wong, 2001). Since shear stress is a function of normal stress (6), baseline parameters for the pressure vs. sinkage parameters (discussed in section 2.1) also impact the shear stress-shear displacement curve.

Table 3: Parameters used to compare a low stiffness, poorly bonded snow to a high stiffness, well bonded snow. The well bonded, high stiffness snow uses the well bonded shear stress-shear displacement model (7) and the Bekker pressure-sinkage model (1). The poorly bonded, low stiffness snow uses the poorly bonded shear stress-shear displacement model (8) and the Preston-Thomas pressure-sinkage model (5). Cells with no number mean that the parameter is not used in the models that describe this type of snow.

Terrain parameters for two different types of snow										
Parameter	k	z_m	k_c	k_{ϕ}	n	c	ϕ	K_s	K_{ω}	K_r
[Units]	$\left[\frac{\mathrm{kPa}}{\mathrm{m}}\right]$	[cm]	$\left[\frac{kN}{m^{n+1}}\right]$	$\left[\frac{kN}{m^{n+2}}\right]$	-	[kPa]	[°]	[cm]	[cm]	-
Well Bonded, High Stiffness	-	-	2.49	246	1.6	6.0	23	-	2.2	0.66
Poorly Bonded, Low Stiffness	19.2	54	-	-	-	0.6	9	5.0	-	-

Ultimately, all the terrain parameters are linked, and independently forcing individual parameters to the extremes of their measured ranges yields incongruous results. For example, a well bonded snow would not likely have a shallow pressure-sinkage curve. Similarly, a poorly bonded snow would not, by definition, have high cohesion or a steep angle of internal friction. Therefore, the poorly bonded shear model is only applied to low cohesion and low stiffness snowpacks, and the well bonded model is only applied to high cohesion and high stiffness snowpacks. The wide range of tractive forces that can be achieved by a wheel operating on these two, very different types of snow is illustrated in Fig. 3, with Table 3 showing the relevant parameters for each curve presented. This plot further demonstrates the range of possible snow variants and the resulting difficulty in optimizing a wheel to gain traction in all conditions.

2.3. Balance of Forces

These simplified models of pressure versus sinkage and shear stress versus shear displacement allow us to calculate drawbar pull and trafficability of the vehicle given certain assumptions. The first assumption is that the two-dimensional normal and shear stress distributions along the rim of the wheel are uniform across the width of the wheel. The second is that the robot is

traveling at a constant velocity and static equilibrium conditions hold. The balance of forces can then be described by

$$W = r_w b \left[\int_{\theta_2}^{\theta_1} \sigma(\theta) \cos \theta d\theta + \int_{\theta_2}^{\theta_1} \tau(\theta) \sin \theta d\theta \right]$$
 (10)

$$F_x = r_w b \left[\int_{\theta_2}^{\theta_1} \tau(\theta) \cos \theta d\theta - \int_{\theta_2}^{\theta_1} \sigma(\theta) \sin \theta d\theta \right]$$
 (11)

$$T_r = r_w^2 b \int_{\theta_2}^{\theta_1} \tau(\theta) d\theta \tag{12}$$

where W is the weight of the robot, F_x is the drawbar pull, and T_r is the resistive torque. The first equation (10) defines the amount of sinkage the robot wheels experience by balancing the force exerted on the wheels by the terrain with the normal force of the robot. With this sinkage known, the shear force that can be applied by the wheel before terrain failure can be calculated (first term of Eq. (11)). This force must be greater than the compaction resistance force in opposition to the robot's motion (second term of Eq. (11)) in order for drawbar pull to be positive and for the robot to successfully traverse the terrain. The resistive torque (12) is the minimum torque that must be transmitted to the wheels to overcome the terrain resistance forces.

2.4. Other Factors

While these are the basic equations for predicting vehicle mobility, other factors need to be considered. Another force acting against the motion of the robot is known as bulldozing resistance. The portion of a driven wheel in the forward flow regime of the soil discovered by Wong and Reece (1967a), can be approximated by a blade pushing against the soil (Wong, 2001). The soil experiences local shear failure and exhibits a resistive force equal to

$$R_b = b \left(0.667 \, z_0 \, c \, K_c + 0.5 \, z_0^2 \, \gamma \, K_y \right) \tag{13}$$

where b is the wheel width, z_0 is the distance in the z-axis from the terrain surface to the transition point of the two flow regimes, c is cohesion, γ is the soil specific weight (set to 1.96 kN/m³), and K_c and K_y are soil bearing capacity factors, calculated from Terzaghi's factors, N_c and N_y (Terzaghi, 1943; Gee-Clough, 1978). This added term of bulldozing resistance is marginal with small sinkages but becomes important in calculating drawbar pull with the potential of encountering low stiffness, highly compressible snow.

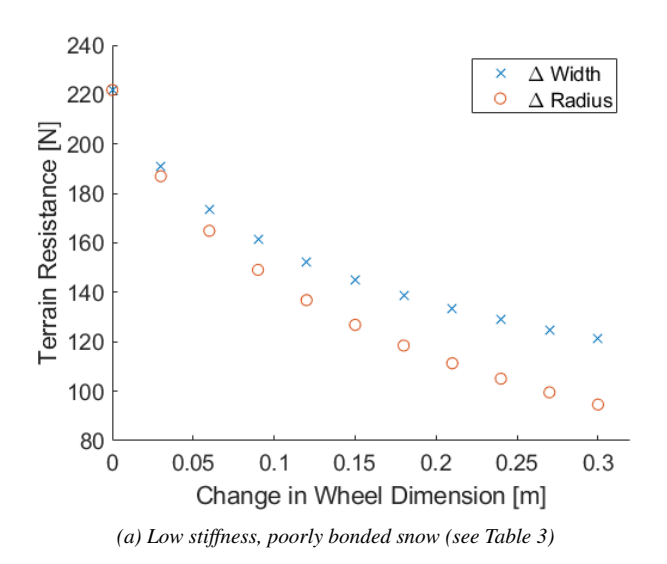
The dynamic effects of sinkage induced from wheel slip is also not captured in the equilibrium equations above. This can be seen when the wheels start to excavate the terrain with increased slip, sinking further and thus increasing compaction resistance. One formula developed to describe this effect has been validated in sands and clays

$$z_{actual} = z_0 + iSz_s \tag{14}$$

where i is the slip and z_0 is the sinkage that would occur were there no excavation (calculated using Bekker's pressure-sinkage relationship (1)), and S is the slip-sinkage coefficient calculated to be approximately 60%/30% (Lyasko, 2009). Lyasko (2009) showed this relationship to be accurate for wheel slips up to 33%, increasing sinkage an additional 60% with prediction errors using this model to be less than 5%. This theory was developed through single-wheel studies in soil, specifically Lunar soil simulant, but the same general principles can be expected to occur in dry snow as well. The larger issue with Lyasko's (2009) models for slip-sinkage is that they do not address how the added sinkage changes the pressure distribution below the wheel, meaning that the equilibrium equations above cannot be solved. Therefore, while these equations are not used directly in calculating improvements that can be made to the tractive elements of the snow rovers, knowing that slip-sinkage is directly linked to predicted sinkage and has a high potential for immobilizing the robot renders the limiting of predicted sinkage a primary objective.

3. New Wheel Design

The main goal of modifying the wheel design of the robot is to increase drawbar pull to reduce the chances of immobilization when towing a load. Increasing drawbar pull is a combination of increasing the shear force applied to the terrain and



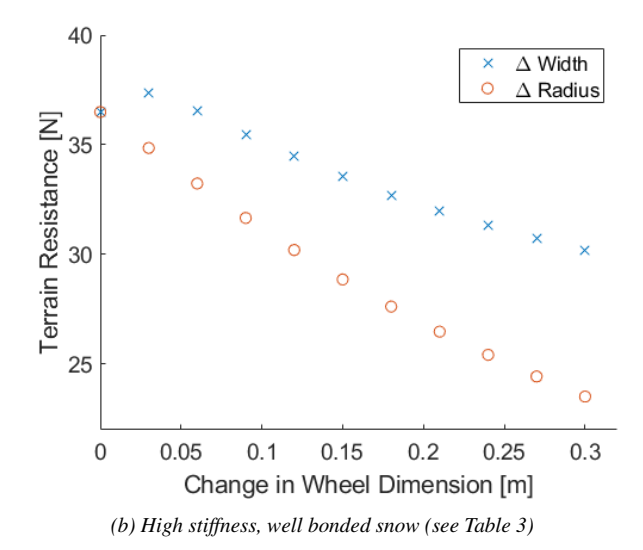


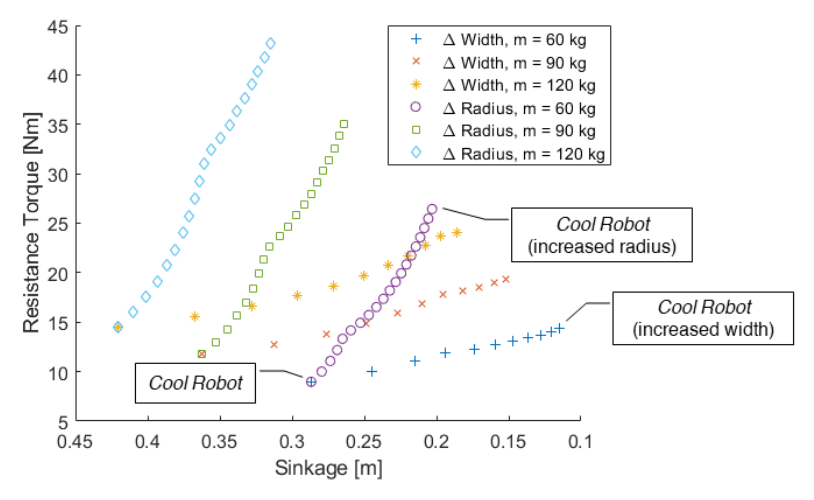
Figure 4: Modeled decrease in compaction resistance of a single wheel with changes in the wheel's dimensions. Wheel width, b, increases from 0.1 m to 0.4 m. Radius, r_w , increases from 0.2 m to 0.5 m. All other variables, including the assumed 60 kg mass of the rover, are kept constant.

decreasing the resistive forces of compaction resistance and bulldozing. To increase shear force, one can either increase the weight of the robot or increase the size of the contact patch. Increasing the weight causes more sinkage and therefore higher compaction resistance, bulldozing, and slip-sinkage (Eq. (14)), so it should be minimized in whatever design changes are implemented. Increasing the contact patch by increasing the width or radius of the wheel is the clear choice but understanding which parameter to vary and how it affects compaction and bulldozing resistance is more complex.

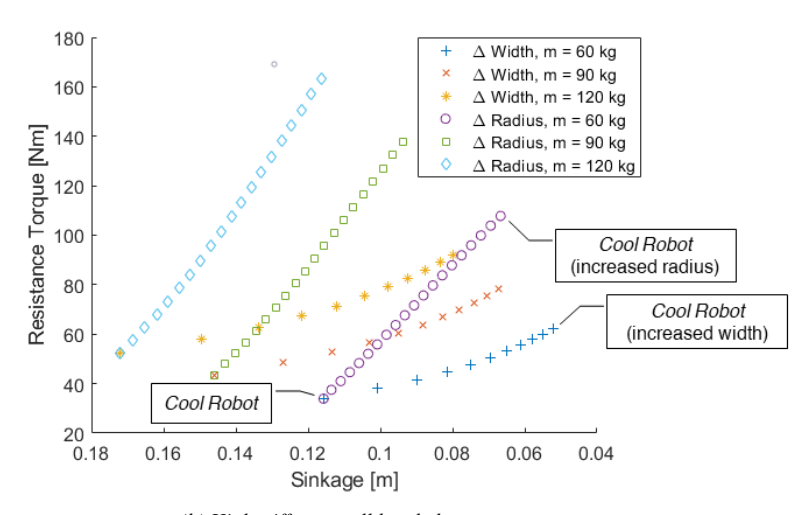
To evaluate the effects of altering wheel dimensions on the rover's trafficability, the terramechanics equations outlined in the previous sections are used with the range of terrain parameters defined in section 2.1 and 2.2. Evaluating all combinations of the different models and parameter values found for snow with each combination of wheel width and radius would be an intractable problem and would only allow for optimization of the wheel dimensions for one type of snow. Therefore, only a worst and best case set of snow parameters, defined by their effect on the rover's mobility, are used to understand the impact of changing the wheel width and the wheel radius. The list of parameter definitions for these two types of snow was presented in Table 3, with the worst snow having high sinkage for a given pressure, employing the poorly bonded model for shear stress-shear displacement, and using the lowest values in the measured range of cohesion and internal friction angle. In contrast, the best snow is that defined by high stiffness, low sinkage, the well bonded traction model, and the highest measured values for cohesion and internal friction angle. The values for c_1 , c_2 , θ_2 , slip ratio, and the inputs to the bulldozing equation (13) remain constant for both snow conditions.

The literature suggests that increasing the radius of the wheel reduces terrain resistance more effectively than increasing wheel width (Wong, 2001; Wallace and Rao, 1993). Terrain resistance is calculated using Eq. (10), where the normal pressure distribution is defined by Eq. (3) and (4) and the shear stress is defined by Eq. (7), (8), and (9). These equations allow for sinkage to be determined for a four-wheeled, 60 kg robot in snow and for the resultant resistance to forward motion applied by the terrain to each wheel to be calculated. Starting from wheel dimensions that roughly correspond to those of the pneumatic tires on *Cool Robot* and *Yeti*, the terrain resistance is compared for an increase in width of 0.3 m to an increase in radius of 0.3 m. Figure 4 shows the relative decrease in the terrain resistance forces given these design changes for two cases, with Fig. 4a using the worst case snow parameters and Fig. 4b using the best case snow parameters. Both graphs show the same trend predicted by Wong (2001) and Wallace and Rao (1993), with an increase in a wheel's radius proving more effective in reducing terrain resistance than an increase in the wheel's width by the same dimension, given a constant load on the wheel.

This direct comparison of terrain resistance for one-to-one changes in radius and width is not particularly useful. These graphs capture no part of the predicted sinkage, which has been shown to have a large impact on slip-sinkage effects, no indicator of drawbar pull, which takes into account the increased shear force as well as both compaction resistance and bulldozing forces, and nothing of the torque required, which would define the motor sizing and energy usage. Therefore, more useful evaluations of changes to radius and width are presented in Figs. 5 and 6 for the two types of snow.



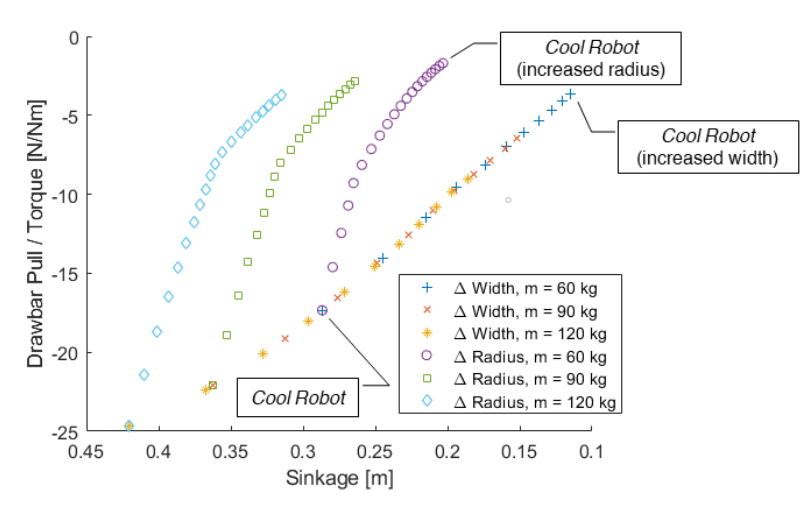
(a) Low stiffness, poorly bonded snow parameters



 $(b) \ High \ stiffness, \ well \ bonded \ snow \ parameters$

Figure 5: Effect of changing wheel dimensions on resistance torque in two different snow types. In both figures, the wheel width, b, was increased from 0.1 m to 0.5 m and the wheel radius, r_w , was increased from 0.2 m to 0.5 m. Note that the x-axis scale is reversed, with left to right corresponding to a decrease in sinkage and an increase in wheel dimensions. Three different robot masses, m, were evaluated, seeing as changing wheel radius or wheel width would impact the rover's mass.

Figures 5a and 5b show how changing the width of the wheel, *b*, decreases sinkage for a given increase in resistive torque far more effectively than increasing the radius of the wheel. This is important in sizing the motor and gearbox for the robot. Increasing the radius of the wheel would almost certainly require a larger motor to handle the higher torques and could potentially require a lengthening of the chassis, resulting in an increase in body weight as well as wheel weight, without a significant decrease in sinkage. On the other hand, increasing the width of the wheel (especially in low stiffness, low cohesion snow), has a drastic impact on reducing sinkage and is less likely to necessitate upsizing the motor. The only impact on weight would be the heavier wheels. The second set of graphs (Figs. 6a and 6b) shows how much the increase in torque, given a change in wheel dimensions, translates to a change in drawbar pull by introducing a new variable called the *mobility efficiency* factor. Instead of normalizing drawbar pull by vehicle weight, as is done with the traction coefficient, the mobility efficiency factor normalizes the drawbar pull by the resistive torque to evaluate the 'usable' torque given a design change in the wheel geometry. For the low stiffness, low cohesion terrain, increasing the radius of the wheels has a more pronounced impact on the mobility efficiency, but the wider wheels can achieve the same drawbar pull per torque specification as the large radius wheels with lower sinkage. Also, for the high stiffness, high cohesion terrain, increasing the radius can actually decrease the mobility efficiency factor, whereas increasing the width increases this factor while also reducing the wheel's sinkage to a



(a) Low stiffness, poorly bonded snow parameters

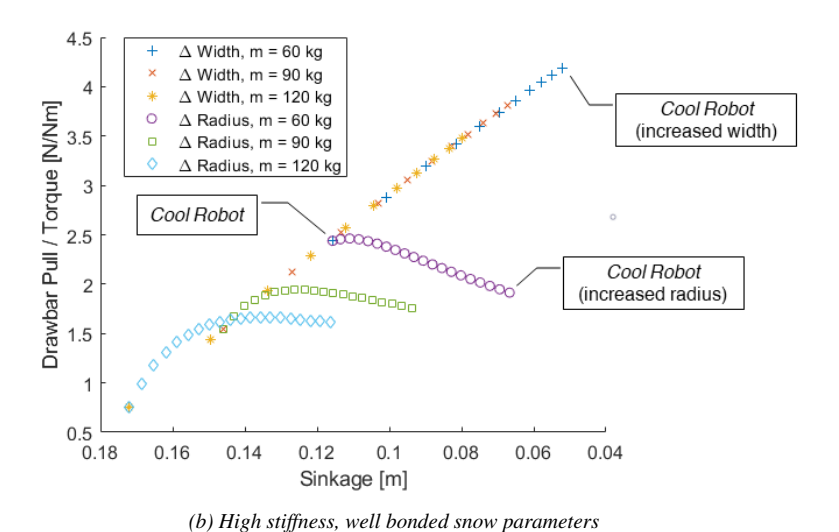


Figure 6: Effect of changing wheel dimensions on the mobility efficiency factor (drawbar pull per torque required [N/Nm]) in two different snow types. In both figures, the wheel width, b, was increased from 0.1 m to 0.5 m and the wheel radius, r_w , was increased from 0.2 m to 0.5 m. Note that the x-axis scale is reversed, with left to right corresponding to a decrease in sinkage and an increase in wheel dimensions. Three different robot masses, m, were evaluated, seeing as changing wheel radius or wheel width would impact the rover's mass.

greater degree.

For all these reasons, it was decided that the redesigned wheels should have increased width rather than drastically increased diameter. The wheels of *Cool Robot* and *Yeti* only have a radius of 0.225 meters with an effective width of approximately 0.12 meters. Based on the results shown in Fig. 6, the new wheels were designed to have a slight increase in radius to 0.265 meters and almost a 4x increase in width, to be 0.45 meters wide. The same motor and gearbox that were used in *Yeti* are used with the new wheels due to the relatively small increase in predicted torque and the wheel weight staying approximately the same at 6 kg each. However, the shafts, bearings, and bearing blocks increased in mass to support the cantilevered load. A front axle pivot was added, giving the robot $\pm 9^{\circ}$ of rotation about the yaw axis to reduce lateral bulldozing resistance in a skid-steer turn and to limit the impact of wider wheels on the rover's maneuverability. All told, the new robot, called *FrostyBoy*, increased in weight from *Cool Robot*'s \sim 60 kg to approximately 90 kg. Even with this increase in mass, the predictions shown in Fig. 6 show an overall reduction in compaction resistance, an increase in drawbar pull, and a decrease

in sinkage.

With such a wide wheel, bulldozing resistance becomes a larger factor in the overall resistance to motion. To counteract this force, grousers were added to the rim of the wheel to reduce the forward flow of the snow. It has been shown that if the grousers interact with the soil before the wheel rim, marginal forward soil flow occurs (Inotsume et al., 2019). While this study was performed in Lunar regolith simulant, the grouser count formula was used to evaluate the design of the new wheel operating in snow

$$n_g > \frac{2\pi(1-i)}{\sqrt{(1-\hat{h})^2 - (1-\hat{z})^2} - \sqrt{1 - (1-\hat{z})^2}}$$
(15)

with n_g being the minimum number of grousers to fully reduce the forward flow regime resistance, i being slip, and \hat{h} and \hat{z} , the height of the grouser and sinkage, respectively, normalized to the radius of the wheel. Off-the-shelf parts dictated the height of the grouser to be about 5% of the wheel radius and the overall geometry resulted in the wheel having 68 grousers. According to the equation above, this combination of \hat{h} and n_g , along with the approximate projected sinkage of 0.15 m for a 90 kg robot with a wheel width of 0.45 m (see Fig. 6) results in reduced bulldozing resistance for all values of wheel slip and minimum resistance for slips greater than 30%.



Figure 7: Prototype of new wheel design

These models were used to inform the final design and prototypes of the new wheels. As can be seen in Fig. 7, the new wheel is made up of two aluminum sidewalls, rigidly mounted to a shaft, with the outer diameter of the wheel being formed by aluminum U-channel grousers. The open sidewalls and gaps between grousers prevent snow from accumulating in the drum of the wheel, keeping it light and balanced.

4. Testing Results

These models serve well in predicting general trends in how modifying wheel dimensions impacts mobility and energy usage for a single wheel in low stiffness, low cohesion snow, but to truly assess any performance improvements, the four-wheeled rover needs to be tested *in situ*. To qualitatively test these prototype wheels, *FrostyBoy* was operated in the dry snow zone of Greenland in 2018. In over 80 km of towing an 80 kg sled of GPR equipment, the robot never became immobilized and was observed to have significantly less sinkage compared to *Cool Robot*, which averaged one immobilization per kilometer when operating the year prior in the same location. Since snow conditions vary drastically from year to year and from month to month in Greenland and since no plate indentation or shear ring tests were performed, it is impossible to directly compare the number of immobilizations in 2017 with the lack thereof in 2018. However, the ability to tow a heavier sled for a significantly



Figure 8: Photo of FrostyBoy taken from behind the rover after an immobilization event in Lebel-sur-Quévillon.

longer distance with zero immobilizations gives an idea of the improved performance. The wider wheels, combined with the front axle pivot, were also proven not to have a significant impact on maneuverability, as FrostyBoy was able to meet the minimum turning radius (\sim 5 m) necessary to replicate tight GPR survey grids performed with $Cool\ Robot$. The sinkage of the wheels, relative to that observed for a snowmobile and a human on the same patch of snow, allows for direct comparison of surface pressure. FrostyBoy was observed to sink less than a snowmobile track (\sim 3.5 kPa) in snow where normal boot pressure (\sim 60 kPa) causes sinkage of about 3 to 4 cm. In addition, when FrostyBoy was driven up an incline of about 20° during the 2018 field season, the motors reached a current limit on the motor controllers that translates to approximately 40 Nm per wheel, meaning they were limited by the motor controllers and not by a limitation in their ability to gain traction, as no wheel slip was observed.

To test the wheels' impact on the rover's mobility quantitatively, FrostyBoy was outfitted with proprioceptive sensors and operated in low stiffness, low cohesion snow on a frozen lake in Lebel-sur-Quévillon, Québec, Canada in March of 2020. The terrain was characterized by plate-indentation measurements (labeled Preston 2 through Preston 5 in Fig. 2) showing that the test-site snow is highly variable and serving as the low stiffness parameters in the pressure-sinkage models used above. To test FrostyBoy's mobility, all four motors were sent the same open loop voltage command. Measurements of robot ground speed, motor currents, motor speeds, and longitudinal and lateral accelerations were logged during each run. This dataset is missing a large number of critical measurements to allow for direct comparison with the calculations shown in Fig. 6 (no direct measurements of sinkage due to malfunctioning ultrasonic sensors, no measurement of internal friction angle, cohesion, shear deformation modulus, c_1 , c_2 , etc.). Many of these parameters can only be accurately determined in single-wheel studies with expensive multi-axis sensors or video particle tracking systems and only for tightly controlled, homogeneous terrains. Instead, this limited dataset points to the importance of taking into account the interactions of all four wheels with the terrain and the resulting dynamics, as this appears to have a significant impact on the rover's mobility in snow. FrostyBoy became immobilized countless times during these tests in Lebel-sur-Quévillon, but for a given immobilization event, the mode of failure was not consistent for all four wheels. Instead, in every immobilization, two of the wheels' torques increased and their speeds decreased until they reached a stall condition, while the other two wheels' speeds increased and their torques decreased, approaching 100% slip as the robot came to a halt. Figure 8 shows the rover after becoming immobilized in one of these events and Fig. 9 shows the corresponding proprioceptive sensor data from this event, where the front right and rear left wheels stalled and the front left and rear right wheels reach high levels of slip. The excavation behind the front left and rear

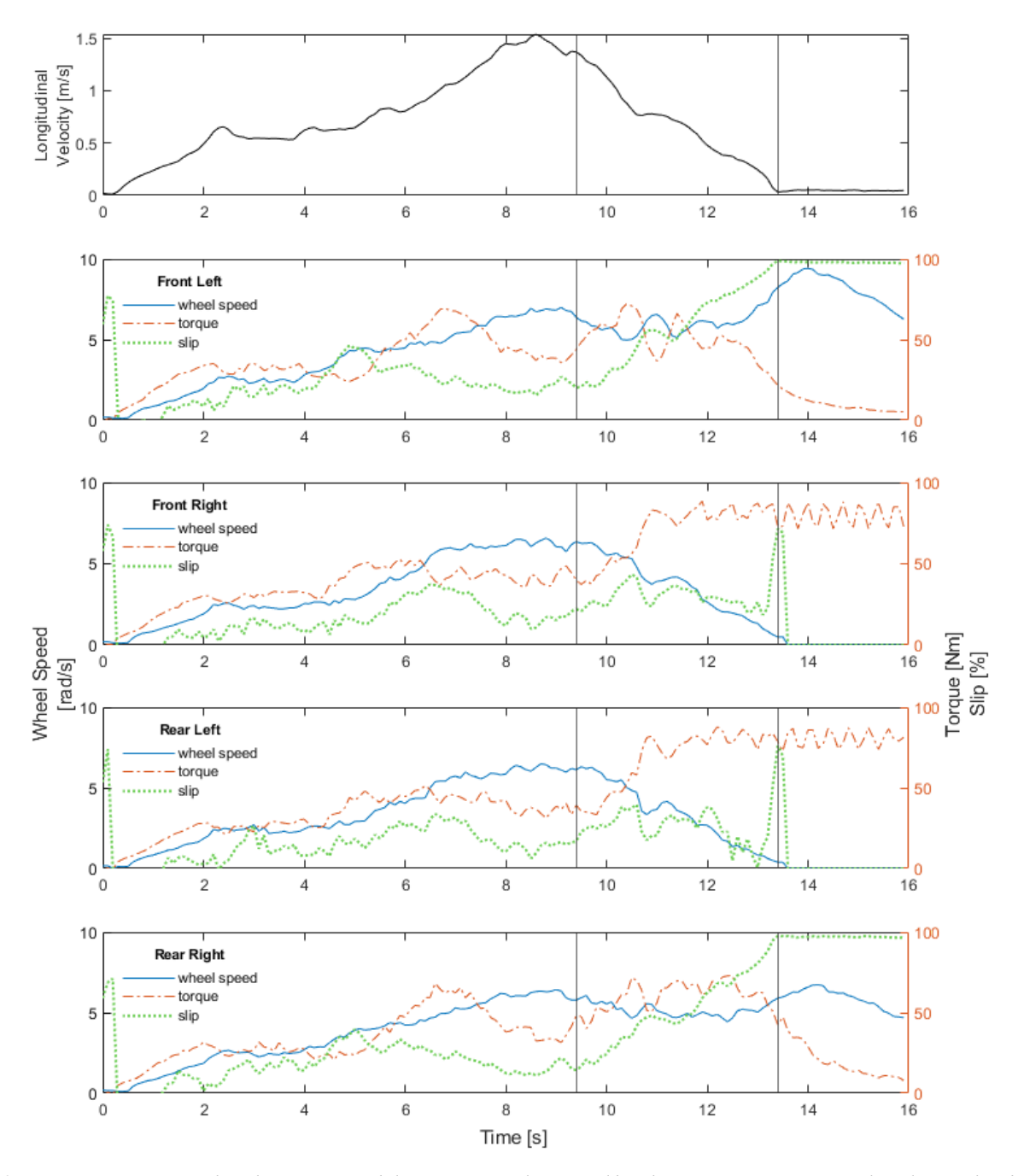


Figure 9: Proprioceptive sensor data during an immobilization event. The vertical bands serve as registration marks to line up data between wheels and roughly mark the period in which FrostyBoy lost mobility.

right wheels also point to the importance of further developing dynamic slip-sinkage models. More importantly, this mode of failure exposes the need for further investigation into the largely unexplored interplay of vehicle dynamics and spatially varying terrain parameters impacting mobility.

The high rate of immobilization events during testing in Lebel-sur-Quévillon might appear to invalidate the design improvements made using terramechanics theory. However, the majority of snow in Greenland and Antarctica is not like that encountered in Lebel-sur-Quévillon. This is evidenced by looking at the years of *Cool Robot*'s and *Yeti*'s successful campaigns towing sensors in these locations, operating over longer distances with much higher ground pressure compared to

FrostyBoy but with fewer immobilization events. Instead, these data serve as a high concentration of information about a small percentage of snow conditions that would typically be encountered on a traverse. However, they require further study seeing as a single patch of low stiffness or low cohesion snow could put an end to a traverse even when the rover is outfitted with wheels designed for lower sinkage and higher traction.

5. Conclusion

The Bekker-Wong terramechanics theory can provide a useful framework in guiding the design of tractive elements to increase mobility in deformable terrain. However, this analysis should not rely on comparing the impact of changing radius or width on only the one factor of compaction resistance. Instead, the impact on the entire system needs to be considered, taking into account how increasing torque affects sizing of the motor, the energy required to traverse a given distance, and evaluating if it is effective in increasing drawbar pull using the *mobility efficiency* factor. Also, one needs to consider how changes in the wheel dimensions can have ballooning effects on the vehicle's weight, with heavier components to handle the increased stresses and a potentially larger chassis to accommodate the larger wheel radius. Similarly, this comprehensive approach is shown to be necessary in evaluating a vehicle's mobility as well. While modifying the tractive elements of the robot was shown to drastically reduce the chances of immobilization, the terramechanics theory developed in isolated and controlled single-wheel studies is not sufficient in predicting a rover's mobility. Instead, further investigation in the feedback between changing terrain parameters and the resulting vehicle dynamics is required to refine the design process in developing an autonomous snow rover.

Acknowledgements

This work was supported by the National Science Foundation's (NSF) Division of Civil, Mechanical and Manufacturing Innovation's (CMMI) program for Dynamics, Control and Systems Diagnostics' (DCSD) award #1824687.

References

- Bekker, M.G., Gregory, M.G.M., 1956. Theory of Land Locomotion: The Mechanics of Vehicle Mobility. Ann Arbor, MI, USA: The University of Michigan Press.
- Gee-Clough, D., 1978. The effect of wheel width on the rolling resistance of rigid wheels in sand. Journal of Terramechanics, 15(4), 161–184.
- Haehnel, R.B., Shoop, S.A., 2004. A macroscale model for low density snow subjected to rapid loading. Cold Regions Science and Technology, 40(3), 193–211.
- Inotsume, H., Moreland, S., Skonieczny, K., Wettergreen, D., 2019. Parametric study and design guidelines for rigid wheels for planetary rovers. Journal of Terramechanics, 85, 39–57.
- Ishigami, G., Nagatani, K., Miwa, A., Yoshida, K., 2007. Terramechanics-based model for steering maneuver of planetary exploration rovers on loose soil. Journal of Field Robotics, 24(3), 233–250.
- Jayakumar, P., Melanz, D., Maclennan, J., Gorsich, D., Senatore, C., Iagnemma, K., 2014. Scalability of classical terramechanics models for lightweight vehicle applications incorporating stochastic modeling and uncertainty propagation. Journal of Terramechanics, 54, 37–57.
- Lever, J.H., 2007. Over-snow rolling resistance of wheeled vehicles. In: International Society for Terrain-Vehicle Systems. Fairbanks, Alaska.
- Lyasko, M., 2009. Slip sinkage effect in soil-vehicle mechanics. Journal of Terramechanics, 47, 21–31.
- Moreland, S., Skonieczny, K., Inotsume, H., Wettergreen, D., 2012. Soil behavior of Wheels with Grousers for Planetary Rovers. In: IEEE Aerospace Conference. Big Sky, MT, USA.

- Nagatani, K., Ikeda, A., Sato, K., Yoshida, K., 2009. Accurate estimation of drawbar pull of wheeled mobile robots traversing sandy terrain using built-in force sensor array wheel. In: IEEE RSJ International Conference on Intelligent Robots and Systems. pp. 2373–2378.
- Quincey, D.J., Luckman, A., 2009. Progress in satellite remote sensing of ice sheets. Progress in Physical Geography, 33(4), 547–567.
- Ray, L., Adolph, A., Morlock, A., Walker, B., Albert, M., Lever, J.H., Dibb, J., 2014. Autonomous rover for polar science support and remote sensing. In: International Geoscience and Remote Sensing Symposium (IGARSS). pp. 4101–4104.
- Ray, L.E., 2009. Estimation of terrain forces and parameters for rigid-wheeled vehicles. IEEE Transactions on Robotics, 25(3), 717–726.
- Rivera, Z.B., De Simone, M.C., Guida, D., 2019. Unmanned ground vehicle modelling in Gazebo/ROS-based environments. Machines, 7(2), 1–21.
- Senatore, C., Iagnemma, K., 2014. Analysis of stress distributions under lightweight wheeled vehicles. Journal of Terramechanics, 51(1), 1–17.
- Shepherd, A., et al., 2012. A reconciled estimate of ice-sheet mass balance. Science, 338, 1183–1190.
- Shoop, S., Kestler, K., Haehnel, R., 2006. Finite element modeling of tires on snow. Tire Science and Technology, 34(1), 2–37.
- Sommerfeld, R.A., LaChapelle, E., 1970. The classification of snow. Journal of Glaciology, 9(55).
- Terzaghi, K., 1943. Theoretical Soil Mechanics. New York, NY, USA: John Wiley and Sons, Inc.
- Trautmann, E., Ray, L., Lever, J., 2009. Development of an autonomous robot for ground penetrating radar surveys of polar ice. In: IEEE/RSJ International Conference on Intelligent Robots and Systems. St. Louis, MO, USA: IEEE. pp. 1685–1690.
- Trease, B., Arvidson, R., Lindemann, R., Bennett, K., Zhou, F., Iagnemma, K., Senatore, C., Van Dyke, L., 2011. Dynamic Modeling and Soil Mechanics for Path Planning. In: Proceedings of the ASME 2011 International Design Engineering Technical Conferences & Computers and Information in Engineering Conference. pp. 1–11.
- Wallace, B.E., Rao, N.S., 1993. Engineering elements for transportation on the lunar surface. Applied Mechanics Reviews, 46(6), 301–312.
- Wong, J.Y., 2001. Theory of Ground Vehicles. 3rd ed. New York, NY, USA: John Wiley and Sons, Inc.
- Wong, J.Y., Preston-Thomas, J., 1983. On the characterization of the pressure-sinkage relationship of snow covers containing an ice layer. Journal of Terramechanics, 20(1), 1–12.
- Wong, J.Y., Reece, A.R., 1967a. Prediction of rigid wheel performance based on the analysis of soil-wheel stresses. Part I. Performance of driven rigid wheels. Journal of Terramechanics, 4(1), 81–98.
- Wong, J.Y., Reece, A.R., 1967b. Prediction of rigid wheel performance based on the analysis of soil-wheel stresses. Part II. Performance of towed rigid wheels. Journal of Terramechanics, 4(2), 7–25.